Anisotropy of Sheared Carbon-Nanotube Suspensions

D. Fry,[1] B. Langhorst,[1] H. Kim,[2] E. Grulke,[3] H. Wang,[4] and Erik K. Hobbie[1,*]

[1]*National Institute of Standards and Technology, Gaithersburg, Maryland 20899, USA*
[2]*Department of Chemistry, Kyunghee University, Yongin, Kyungkido, 449-701, Korea*
[3]*Department of Chemical Engineering, University of Kentucky, Lexington, Kentucky 40506, USA*
[4]*Department of Materials Science and Engineering, Michigan Technological University, Houghton, Michigan 49931, USA*
(Received 21 July 2004; published 15 July 2005)

We measure the anisotropy of sheared carbon-nanotube suspensions for a broad range of concentration, aspect ratio, and strain rate using a variety of methods. Our measurements highlight the importance of excluded-volume interactions in the semidilute regime, with scaling in terms of a dimensionless shear rate. Our results also suggest that such interactions might be exploited to fractionate carbon nanotubes by length in simple shear flow.

DOI: 10.1103/PhysRevLett.95.038304 PACS numbers: 82.70.−y, 47.55.Kf, 61.46.+w

Carbon nanotubes exhibit remarkable physical properties and there is considerable interest in using them as nanoscale building blocks for a new generation of materials and applications [1–6]. Despite this promise, fundamental issues related to the dispersion, fractionation, orientation, and manipulation of individual nanotubes remain unresolved and efficient bulk processing schemes do not exist. Single-walled carbon nanotubes (SWNTs), for example, have strong van der Waals attractions that inhibit nematic ordering in surfactant-stabilized suspensions [7], and routes to liquid crystallinity have thus far required volume compression [7] or dispersion in superacid solvents [8]. Multiwalled carbon nanotubes (MWNTs) are easier to disperse, but flow instabilities related to mechanical entanglement hinder processibility [9] and the tubes must be shortened considerably to achieve a nematic phase [10].

In light of these issues, establishing routes to proficient processing will depend in part on a detailed understanding of the response of carbon-nanotube dispersions to changes in such parameters as composition, temperature, aspect ratio, and shear stress. In this Letter, we use a variety of methods to measure the anisotropy of sheared carbon-nanotube suspensions over the entire semidilute regime. Our measurements highlight the importance of excluded-volume interactions, with scaling over a broad range of reduced strain rate, or Peclet number. Our results also suggest how these interactions might be exploited to fractionate carbon nanotubes by length in simple shear flows.

SWNTs synthesized *via* the high-pressure catalytic decomposition of carbon monoxide (HiPCO) were obtained commercially. They were purified through thermal oxidation at 260 °C, refluxing in HCl solution, and ultrasonication in nitric acid. Suspensions were made by sonicating purified SWNTs in 0.6% by mass sodium dodecylbenzenesulfonate (SDBS) D_2O solution, which has been shown to be an effective means of preparing stable aqueous SWNT dispersions [11]. After cold ultrasonication for 10 h, the tubes exist in suspension as SWNT ropes. Atomic-force microscopy (AFM) of dried films gave a mean diameter (d) of 13.5 nm and a mean length (L) of 0.75 μm ($L/d \approx 60$). Further processing led to less detectable anisotropy in shear flow. We focus on 0.08% and 0.16% SWNT by mass, with $cL^3 \approx 1.7$ and 3.5, respectively, where c is the number of tubes per unit volume. The shear viscosity is $\eta \approx 1$ mPa s, and we denote these suspensions S1.

The MWNTs were grown *via* chemical vapor deposition (CVD). Electron microscopy gave $d \approx 50$ nm and the mean length was determined optically to be $L \approx 10$ μm ($L/d \approx 200$). The length distribution is nearly log-normal with a polydispersity of 2. They were suspended in low-molecular-mass polyisobutylene (PIB) fluids as described elsewhere [9,12]. We use two PIB fluids; an elastic Boger fluid ($M_w = 800$ with 0.1% $M_w = 4.7 \times 10^6$, $\eta_0 =$ 10 Pa s) and a Newtonian fluid ($M_w = 500$, $\eta_0 =$ 0.5 Pa s). Suspensions in the former, which we denote M1, were prepared at 0.1% to 0.8% MWNT by mass, with $cL^3 \approx 24$ to 200. Suspensions in the latter, which we denote M2, were prepared at 0.025% to 0.85% MWNT by mass, with $cL^3 \approx 6$ to 210. For both M1 and M2, η is comparable to the solvent viscosity, η_0. For all suspensions, $0.01 < cL^2d < 1$, with our measurements spanning the semidilute regime [13].

We consider linear shear flow along $\hat{\mathbf{x}}$, with a constant velocity gradient along $\hat{\mathbf{y}}$ and vorticity along $\hat{\mathbf{z}}$. The shear rate is $\dot{\gamma} = \partial v_x/\partial y$ and we probe structure in the x-z plane at 25 °C, with pure surfactant suspensions showing negligible anisotropy. Birefringence, dichroism, and η were measured simultaneously as a function of $\dot{\gamma}$ in a 200 μm gap parallel-plate optical shear cell with a 670 nm diode laser. A modulated linear polarization with a lock-in technique was used to extract $\Delta n'$ and $\Delta n''$, the real and imaginary parts of the difference between the largest and smallest eigenvalue of the complex refractive-index tensor in the x-z plane [14]. For S1, small-angle neutron scattering (SANS) measurements were performed on the 8 m SANS instrument at the NIST Center for Neutron Research using a 0.5 mm gap Couette shear cell, with a

wave vector range 0.006 $\text{Å}^{-1} < q < 0.1$ Å^{-1}. For M1 and M2, depolarized small-angle light scattering (SALS) ($\lambda = 632.8$ nm) and stroboscopic video microscopy (SVM) measurements were performed concurrently using a parallel-plate shear cell [15]. Polarization along the x (z) axis is denoted h (v), where SALS probes 0.5 $\mu\text{m}^{-1} < q < 5$ μm^{-1}. SVM images were processed [15] to obtain an approximate uniaxial orientational distribution function (ODF), $p(\theta)$, where θ is the angle a MWNT makes with $\hat{\mathbf{x}}$. We restrict our measurements to shear rates where the suspensions are homogeneous and the tubes are well dispersed [9]. The Reynolds number is $10^{-5} < \text{Re} \lesssim 300$, being >1 only in S1 at high $\dot{\gamma}$. In all cases, the mean shear-induced orientation is along $\hat{\mathbf{x}}$.

In simple shear, the tubes are in any one of a family of closed periodic Jeffery orbits around $\hat{\mathbf{z}}$, with the distribution of these orbits dictating the ODF [16]. The optical anisotropy is $\Delta n = \Delta n' + i\Delta n'' \approx \frac{1}{2}\delta_1 \phi S$, where ϕ is the volume fraction of nanotubes, $\delta_1 = \delta_1' + i\delta_1''$ is the dielectric anisotropy, and $S = \langle P_2(\cos\theta)\rangle = \frac{1}{2}[3\langle\cos^2\theta\rangle - 1]$ is a (para)nematic order parameter, being 0 for a random distribution and 1 for perfect alignment [17]. In this expression, $\delta_1 = \alpha_\parallel - \alpha_\perp$, where $\alpha_\parallel$ and $\alpha_\perp$ are the complex permittivities along and normal to a tube axis. Figure 1 shows the scaled birefringence and dichroism as a function of Peclet number, $\text{Pe} = \dot{\gamma}/D_r$. For dilute rods, the rotary diffusion coefficient is [13]

$$D_r = D_0 = 3k_B T[\ln(L/d) - 0.8]/(\pi\eta L^3), \qquad (1)$$

and Eq. (1) has been used to reduce the S1 data. In the semidilute regime, excluded-volume interactions lead to the rescaling [13,18]

$$D_r = \beta D_0 (cL^3)^{-2} \propto D_0 \phi^{-2}, \qquad (2)$$

where $\beta \approx 1350$, and Eq. (2) has been used to reduce data for M1 and M2 [19]. We find scaling over 10 decades in Pe with no free parameters, the data falling into two distinct groups by type. Although solvent elasticity can enhance flow alignment [20], overlay in M1 and M2 suggests a dominance of viscous hydrodynamics in the suspensions of interest. For the MWNTs, $\Delta n/\phi \propto S \propto \text{Pe}^{0.16}$ implies $S \propto \phi^{1/3}$ at fixed $\dot{\gamma}$, which can be compared to the leading-order ($\text{Pe} < 200$) prediction [18] $S \propto \text{Pe}^{0.25}$.

To extract information about the optical anisotropy of the nanotubes requires knowledge of S. For the SWNT suspensions, we determine this from the anisotropy of the SANS structure factor, $S(\mathbf{q})$, where a typical pattern is shown in Fig. 1(b). Treating the polar intensity variation as an effective ODF, $p_e(\theta)$, we compute S *via* the approximation $\langle\cos^2\theta\rangle \approx \int p_e(\theta)\cos^2\theta d\Omega / \int p_e(\theta) d\Omega$, which gives $0.005 < S < 0.09$ over the measured interval of $\dot{\gamma}$. The magnitude of S reflects the relatively small L/d and dilute nature of the SWNT suspensions. For M1 and M2, we compute S from the effective ODF suggested by ensembles of SVM images [Fig. 1(b)] in the x-z plane [15]. In

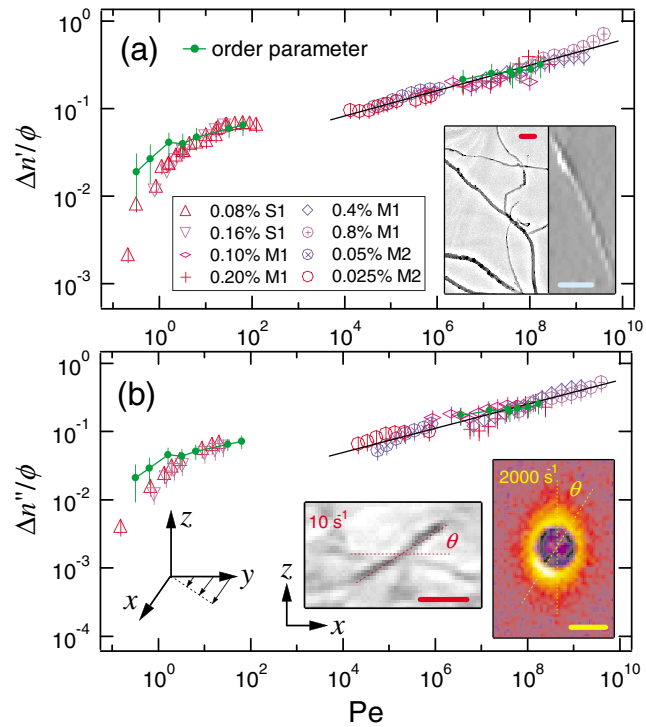

FIG. 1 (color online). (a) Scaled $\Delta n'$ vs Pe, where the left inset is an electron micrograph of the MWNTs and the right inset is an AFM image of the SWNTs (scale bar = 150 nm). The measured S has been scaled onto the data and the line is a power-law fit. (b) Analogous plot of $\Delta n''$, where the left inset is a SVM of a MWNT (scale bar = 5 μm) and the right inset is a SANS pattern for S1 (scale bar = 0.06 nm^{-1}).

this manner, we obtain $0.3 < S < 0.6$, reflecting the larger L/d and semidilute nature of the MWNT suspensions [16]. Multiplying $S(\text{Pe})$ by a constant scales it onto Δn in Fig. 1, providing a measure of δ_1 at $\lambda = 670$ nm. In this manner, we find $\delta_1' \approx 1.5$ and $\delta_1'' \approx 1.65$ for the SWNTs, with $\delta_1' \approx 1.1$ and $\delta_1'' \approx 0.85$ for the MWNTs, consistent with a greater charge mobility parallel to the tube axis. The anisotropy is also larger for the SWNTs, particularly in absorption, indicative of a higher degree of purity. Measurements on aligned metallic SWNTs embedded in a molecular crystal, for example, show strong absorption along the nanotube axis [21].

Although the SWNT suspensions show limited scattering anisotropy in depolarized SALS, M1 and M2 scatter light strongly at low q. In the semidilute regime, the symmetric matrix of structure factors is [17]

$$S_{\mu\nu}(\mathbf{q}) \propto \sum_{l=1}^{N} |(\delta_1)\hat{\mathbf{x}}_\mu \cdot \hat{\mathbf{n}}_l \hat{\mathbf{n}}_l \cdot \hat{\mathbf{x}}_\nu + (\delta_0)\delta_{\mu\nu}|^2 |f_l(\mathbf{q})|^2 \qquad (3)$$

for $(\mu, \nu) = (h, v)$, where $\hat{\mathbf{n}}_l$ is the body director of the lth nanotube, $f_l(\mathbf{q}) = \int_{v_l} e^{-i\mathbf{q}\cdot\mathbf{r}} d\mathbf{r}$, N is the number of tubes, v_l is the volume of the lth tube, and $\delta_0 = \alpha_\perp - \epsilon_s$, with ϵ_s being the dielectric constant of the solvent. The hh scat-

tering is weighted by tubes aligned with $\hat{\mathbf{x}}$, the vv scattering is weighted by tubes aligned with $\hat{\mathbf{z}}$, and the off-diagonal hv term is weighted by tubes aligned off axis, which creates a four-lobed pattern [17]. For a given ODF, $S_{\mu\nu}(\mathbf{q})$ is evaluated numerically.

Figure 2 shows scaled $S_{hh}(\mathbf{q})$ and $S_{vv}(\mathbf{q})$ as a function of ϕ and $\dot{\gamma}$ for M1, where all the data correspond to the same Pe ($S \approx 0.45$). Figure 3 shows an analogous plot of $S_{hv}(\mathbf{q})$ [22]. The bar in the insets is 1 $\mu\mathrm{m}^{-1}$. Scaling of $S_{\mu\nu}(\mathbf{q})$ complements the scaling shown in Fig. 1, and the theoretical curves are projections calculated using the measured L and d. For the fit of $S_{hv}(\mathbf{q})$, we use the Gaussian ODF obtained from a fit of the measured ODF (Fig. 3). Gaussian ODFs describe the anisotropy of directed wormlike chains in nematic solvents [23], and here we include a small background to account for an element of vorticity orientation [16]. The fits of $S_{hh}(\mathbf{q})$ and $S_{vv}(\mathbf{q})$ are obtained *via* variations in this background that fall within the uncertainty of our leading-order treatment. Note that $|\delta_1|^2 \approx 1.93$ from the above analysis, $|\delta_1|^2 \approx |\delta_0|^2$ from SALS on isotropic suspensions [17], and $|n| \approx 1.6$ from reflectivity measurements [15], with the MWNT optical anisotropy being fixed *a priori* at $\alpha'_{\parallel} \approx 2.8$, $\alpha'_{\perp} \approx 1.7$, $\alpha''_{\parallel} \approx 2.15$, and $\alpha''_{\perp} \approx 1.3$, consistent with the lower limit of anisotropy measured for SWNT bundles [24].

The SALS fitting uses a Gaussian approximation for $|f_l(\mathbf{q})|^2$ that smears high-q structure, and both the measured and computed profiles show q^{-1} behavior (Fig. 2), as expected for linear objects with length polydispersity [17]. Cone-and-plate rheological measurements performed on M1 and M2 show a positive first normal stress difference over the relevant range of $\dot{\gamma}$, consistent with at most limited flexure [25]. A slight degree of deformation is evident in SVM images and we note that such a perturbation can decrease the apparent optical anisotropy [17]. We also note that polydispersity and tube deformation (both quenched and stress-induced) can qualitatively account for both the shape of the ODF and the magnitude of S [16].

Finally, we focus on a subtle but striking feature that suggests a potential route toward the flow fractionation of carbon nanotubes by length in simple shear. In the mid semidilute regime (0.1% to 0.2% M1) at modest $\dot{\gamma}$ (5 s^{-1} to 15 s^{-1}, Pe $\approx 10^6$), longer flow-aligned tubes slowly move into the bulk, while shorter tubes move to the shearing surfaces and align with $\hat{\mathbf{z}}$. As shown in Fig. 4, this is apparent in both the SALS patterns, which develop a bulge along $\hat{\mathbf{x}}$ at late t, and the SVM images, which yield histograms of orientation and projected length at different depths within the sample. The ratio of the wall to bulk fractions can be enhanced by lowering the gap, but at around 20 μm—comparable to the length of the longest MWNTs in the suspension—confinement induces irreversible fibrillation, creating macroscopic fibers that exhibit a mean orientation along $\hat{\mathbf{z}}$ but show considerable flexure as they rock back and forth in the x-z plane [Fig. 4(g)]. We suggest that overlap between the Jeffery orbits of longer MWNTs and the walls drives such flow-aligned tubes into the bulk, with tube-tube interactions then driving shorter MWNTs to the walls, where they orient along $\hat{\mathbf{z}}$. The effect might be most pronounced in the mid semidilute regime because caging effects likely start to hinder tube mobility at higher concentrations.

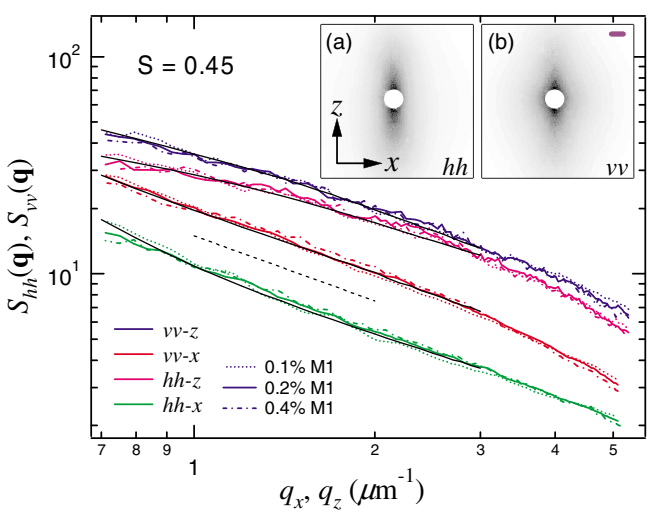

FIG. 2 (color online). Scaled x and z projections of the diagonal elements of $S_{\mu\nu}(\mathbf{q})$, where (a) and (b) are the measured hh and vv patterns for 0.2% M1 at $\dot{\gamma} = 36\ \mathrm{s}^{-1}$. Data for each ϕ correspond to the same Pe, with $S \approx 0.45$. The 0.1% and 0.4% M1 data are at $\dot{\gamma} = 153\ \mathrm{s}^{-1}$ and 9 s^{-1}, respectively. The curves are computed profiles and the line is q^{-1}.

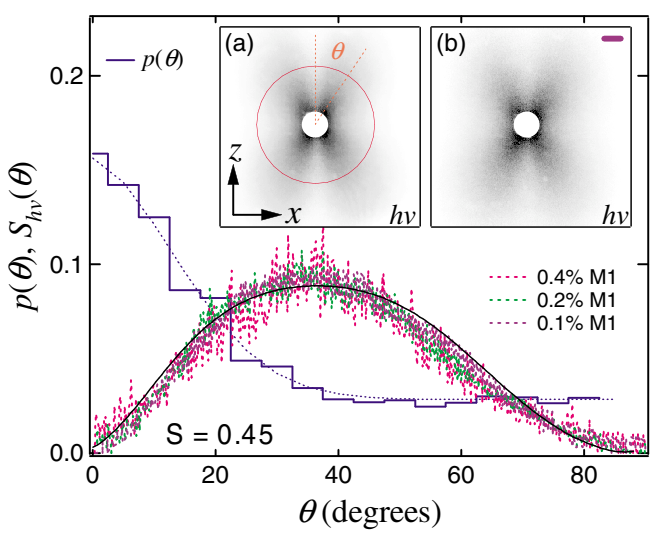

FIG. 3 (color online). Scaled polar projections of the off-diagonal element of $S_{\mu\nu}(\mathbf{q})$, where (a) and (b) are the measured hv patterns for 0.2% M1 at $\dot{\gamma} = 36\ \mathrm{s}^{-1}$ and 0.4% M1 at 9 s^{-1}, respectively. The black curve is the computed profile. The histogram is the ODF measured with SVM and the dashed curve is a Gaussian fit.

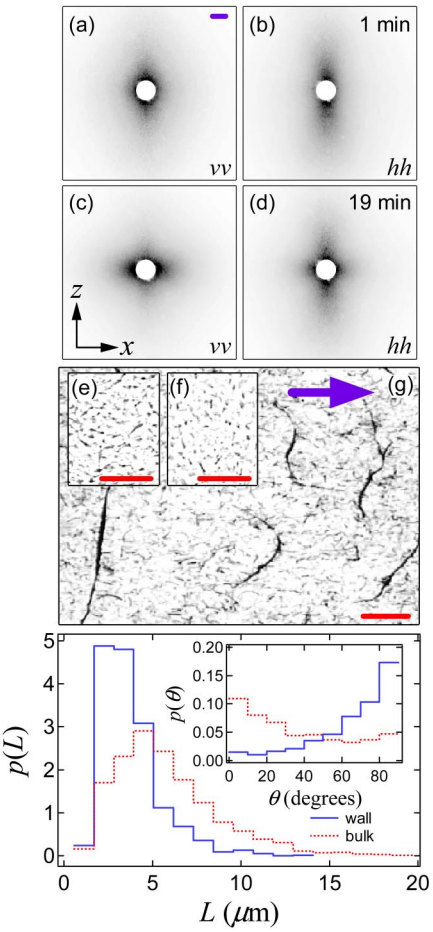

FIG. 4 (color online). The (a) vv and (b) hh patterns for 0.2% M1 at $\dot{\gamma} = 14\ \mathrm{s}^{-1}$, $t = 1$ min, where (c) and (d) show the same at $t = 19$ min. The inset (e) shows a micrograph in the bulk for 0.1% M1 at $\dot{\gamma} = 14\ \mathrm{s}^{-1}$, $t = 19$ min, while (f) shows the same near a wall. As in Figs. 1–3 the gap in (a)–(f) is 200 μm. Lowering the gap to 20 μm leads to irreversible fibrillation, as shown in (g) for 0.2% M1 at $\dot{\gamma} = 100\ \mathrm{s}^{-1}$. The scale bar in (e)–(g) is 25 μm. The lower panel shows projected length and orientation histograms for (e) and (f).

Beyond their potential applications, carbon nanotubes are mesoscale analogs of rigid-rod polymers, and we hope that the measurements presented here will offer valuable insight into the flow-induced anisotropy of such systems. We also hope that our results will contribute to the development of new and efficient methods for sorting large numbers of carbon nanotubes by length.

The authors thank S. Milner, D. Morse, D. Koch, and S. D. Hudson for useful suggestions and fruitful discussions.

*Electronic address: erik.hobbie@nist.gov

[1] T. W. Odom *et al.*, Nature (London) **391**, 62 (1998).
[2] S. Fan *et al.*, Science **283**, 512 (1999).
[3] J. Kong *et al.*, Science **287**, 622 (2000).
[4] M. J. O'Connell *et al.*, Science **297**, 593 (2002).
[5] B. Vigolo *et al.*, Science **290**, 1331 (2000).
[6] R. H. Baughman, A. A. Zakhidov, and W. A. de Heer, Science **297**, 787 (2002).
[7] M. F. Islam *et al.*, Phys. Rev. Lett. **92**, 088303 (2004).
[8] V. A. Davis *et al.*, Macromolecules **37**, 154 (2004).
[9] S. Lin-Gibson *et al.*, Phys. Rev. Lett. **92**, 048302 (2004).
[10] W. Song, I. A. Kinloch, and A. H. Windle, Science **302**, 1363 (2003).
[11] M. F. Islam *et al.*, Nano Lett. **3**, 269 (2003).
[12] The MWNT suspensions contain a succinimide polymer (1:1 MWNT by mass, PIB soluble) as dispersant [C. Park *et al.*, Nanotechnology **14**, L11 (2003)]. There is clustering in weak shear [9], but light scattering and microscopy confirm that the MWNTs are well dispersed at the shear rates of interest here.
[13] R. G. Larson, *The Structure and Rheology of Complex Fluids* (Oxford University Press, New York, 1999).
[14] G. G. Fuller, *Optical Rheometry of Complex Fluids* (Oxford University Press, New York, 1995).
[15] E. K. Hobbie *et al.*, Rev. Sci. Instrum. **74**, 1244 (2003).
[16] See, for example, M. Rahnama, D. L. Koch, and E. S. G. Shaqfeh, Phys. Fluids **7**, 487 (1995); The ODF can exhibit anisotropy in the y-z plane, but our measurements will be insensitive to this.
[17] E. K. Hobbie, J. Chem. Phys. **121**, 1029 (2004).
[18] M. Doi and S. F. Edwards, *The Theory of Polymer Dynamics* (Oxford University Press, New York, 1986).
[19] Although S1 is Brownian, M1 and M2 are not strictly so. Koch has proposed $D_r \propto cL^3\dot{\gamma}$ for semidilute non-Brownian suspensions, where the constant of proportionality depends on L/d [D. L. Koch, Phys. Fluids **7**, 2086 (1995)]. To make a dimensionless group, we reduce D_r by $\tau = (\tau_0/\eta_0)(\eta - \eta_0)$, with τ_0 being any dilute relaxation time (e.g., D_0^{-1} for Brownian tubes). The generalized Peclet number, $D_r\tau \propto cL^3\dot{\gamma}\tau_0[\eta]\phi$ where $[\eta]$ is the intrinsic viscosity, has the same ϕ^2 scaling.
[20] Y. Iso, C. Cohen, and D. L. Koch, J. Non-Newtonian Fluid Mech. **62**, 135 (1996).
[21] Z. M. Li *et al.*, Phys. Rev. Lett. **87**, 127401 (2001).
[22] Projections are scaled with a background and a constant factor. The mean anisotropy of the background is 0.2 and that of the amplitude is 0.07, with 0 being isotropic. At constant gap, the amplitude scales as $\phi e^{-\Gamma_{\mu\nu}\phi}$, as expected for single scattering in an anisotropically absorbing medium, where $\Gamma_{\mu\nu}$ is a constant.
[23] Z. Dogic *et al.*, Phys. Rev. Lett. **92**, 125503 (2004).
[24] Z. Yu and L. Brus, J. Phys. Chem. B **105**, 1123 (2001).
[25] L. E. Becker and M. J. Shelley, Phys. Rev. Lett. **87**, 198301 (2001).